

# Truncation, modification, and optimization of MIG6<sup>segment 2</sup> peptide to target lung cancer-related EGFR



Xiao-Dong Yu<sup>a</sup>, Rui Yang<sup>b</sup>, Chang-Jun Leng<sup>c,\*</sup>

<sup>a</sup> Department of Surgical Oncology, Taizhou Municipal Hospital, Taizhou 318000, China

<sup>b</sup> Linzi District Huangcheng Town Health Center, Zibo 255424, China

<sup>c</sup> Department of Radiotherapy, Linzi District People's Hospital, Zibo 255400, China

## ARTICLE INFO

### Article history:

Received 23 December 2015

Received in revised form 8 February 2016

Accepted 16 February 2016

Available online xxx

### Keywords:

Human epidermal growth factor receptor

MIG6 protein

Peptide

Lung cancer

## ABSTRACT

Human epidermal growth factor receptor (EGFR) plays a central role in the pathological progression and metastasis of lung cancer; the development and clinical application of therapeutic agents that target the receptor provide important insights for new lung cancer therapies. The tumor-suppressor protein MIG6 is a negative regulator of EGFR, which can bind at the activation interface of asymmetric dimer of EGFR kinase domains to disrupt dimerization and then inactivate the kinase (Zhang X. et al. *Nature* 2007, 450: 741–744). The protein adopts two separated segments, *i.e.* MIG6<sup>segment 1</sup> and MIG6<sup>segment 2</sup>, to directly interact with EGFR. Here, computational modeling and analysis of the intermolecular interaction between EGFR kinase domain and MIG6<sup>segment 2</sup> peptide revealed that the peptide is folded into a two-stranded  $\beta$ -sheet composed of  $\beta$ -strand 1 and  $\beta$ -strand 2; only the  $\beta$ -strand 2 can directly interact with EGFR activation loop, while leaving  $\beta$ -strand 1 apart from the kinase. A C-terminal island within the  $\beta$ -strand 2 is primarily responsible for peptide binding, which was truncated from the MIG6<sup>segment 2</sup> and exhibited weak affinity to EGFR kinase domain. Structural and energetic analysis suggested that phosphorylation at residues Tyr394 and Tyr395 of truncated peptide can considerably improve EGFR affinity, and mutation of other residues can further optimize the peptide binding capability. Subsequently, three derivative versions of the truncated peptide, including phosphorylated and dephosphorylated peptides as well as a double-point mutant were synthesized and purified, and their affinities to the recombinant protein of human EGFR kinase domain were determined by fluorescence anisotropy titration. As expected theoretically, the dephosphorylated peptide has no observable binding to the kinase, and phosphorylation and mutation can confer low and moderate affinities to the peptide, respectively, suggesting a good consistence between the computational analysis and experimental assay.

© 2016 Elsevier Ltd. All rights reserved.

## 1. Introduction

Receptor tyrosine kinase (RTK) superfamily represents a subgroup of transmembrane protein receptors that are involved in a variety of developmental processes including cell survival, proliferation and motility, and, when unregulated, play prominent roles in cancer (Lemmon and Schlessinger, 2010). The human epidermal growth factor receptor (EGFR) as an important member of RTK has received particular attention in recent years owing to its strong association with malignant proliferation, which has been shown to play a central role in the development and progression of non-small cell lung cancer (NSCLC) (Bethune et al., 2010). EGFR activation results from the formation of an asymmetric dimer in

which the C-terminal lobe of one kinase domain plays a role similar to that of cyclin in activated CDK/cyclin complexes. The CDK/cyclin-like complex formed by two kinase domains thus explains the activation of EGFR-family receptors by homo- or hetero-dimerization (Zhang et al., 2006). EGFR dimerization stimulates its intrinsic intracellular protein-tyrosine kinase activity. As a result, autophosphorylation of several tyrosine residues in the C-terminal domain of EGFR occurs to elicit downstream activation and signaling by several other proteins that associate with the phosphorylated tyrosines through their own phosphotyrosine-binding SH2 domains.

The mitogen-inducible gene 6 (MIG6) protein has been reported as an important negative regulator of the EGFR signaling by binding at the activation interface of EGFR kinase domain to disrupt EGFR dimerization (Hackel et al., 2001). Accumulated evidences suggest that the MIG6 plays an essential role in suppressing the development, proliferation and metastasis of

\* Corresponding author.

E-mail address: [changjunleng@sina.cn](mailto:changjunleng@sina.cn) (C.-J. Leng).

NSCLC by inactivating EGFR (Zhang et al., 2007a; Maity et al., 2015; Izumchenko and Sidransky, 2015). Knockout of the MIG6 gene has also been found to strongly associate with a variety of tumors such as breast cancer (Wendt et al., 2015), endometrial cancer (Kim et al., 2014) and skin tumor (Ferby et al., 2006). The crystal structure of EGFR–MIG6 complex revealed that two separated segments in MIG6 protein, called MIG6<sup>segment 1</sup> (residues 336–361) and MIG6<sup>segment 2</sup> (residues 376–398), interact with the C-lobe of EGFR kinase domain (Fig. 1) (Park et al., 2015). The binding of MIG6<sup>segment 1</sup> to EGFR activation interface prevents an asymmetric dimer formation, leading to the inhibition of EGFR activation at micromolar binding affinity level (Moonrin et al., 2015). However, the MIG6<sup>segment 1</sup> is only able to inhibit the kinase domain in the context of asymmetric dimer formation, but not directly relevant for shutting down kinase activity. The presence of MIG6<sup>segment 2</sup> C-terminal to MIG6<sup>segment 1</sup> exhibits ability to bind tightly to activated EGFR, which induces the EGFR conformation change from active to inactive states; MIG6<sup>segment 1</sup> alone cannot confer this property, because the kinase residues that interact with it do not change conformation upon activation (Zhang et al., 2007b). Crystallographic analysis revealed that the MIG6<sup>segment 2</sup> can interact directly with activation loop as well as the region close to kinase active site (Park et al., 2015).

Recently, we have successfully designed and optimized several short peptides to target the EGFR family protein HER2 by grafting and truncation of MIG6<sup>segment 1</sup> (Yu et al., 2016). Here, we attempted to systematically investigate the intermolecular interaction between the EGFR kinase domain and MIG6<sup>segment 2</sup> peptide. The isolated MIG6<sup>segment 2</sup> peptide can bind weakly to EGFR kinase domain, and we herein proposed a molecular design scheme to rationally improve its binding capability to EGFR by terminal truncation, structural modification and sequence optimization. We also demonstrated that the scheme can work fairly well by using fluorescence anisotropy assay, and elucidated the molecular mechanism and biological implication underlying the affinity improvement upon the truncation, modification and optimization of MIG6<sup>segment 2</sup> peptide.

## 2. Materials and methods

### 2.1. Molecular dynamics simulation

The EGFR–MIG6<sup>segment 2</sup> peptide complexes were investigated dynamically using molecular dynamics (MD) simulations with AMBER03 force field (Duan et al., 2003). Phosphotyrosine parameters were derived from the AMBER parameter database (Steinbrecher et al., 2012). A solvent box filled with TIP3P water molecules (Jorgensen et al., 1983) was added with a 10 Å buffer around the complex. Counter-ions were employed to neutralize excessive formal charges in the simulated system. First, the system was heated from 0 to 300 K over 100 ps. Then, the simulations were performed in NPT ensemble at a constant temperature of 300 K and a constant pressure of 1 atm. The time step was set to 2 fs. The SHAKE method (Ryckaert et al., 1977) was used to constrain all covalent bonds involving hydrogen atoms, the PME algorithm (Darden et al., 1993) was utilized to calculate the full electrostatic energy in a macroscopic lattice of repeating images, and a cut-off distance of 10 Å was applied for van der Waals interactions. The whole simulations were carried out for 20 ns, and snapshots were saved every 100 ps over the last 10-ns simulations, totally yielding 100 snapshots.

### 2.2. Binding free energy calculation

The molecular mechanics/Poisson–Boltzmann surface area (MM/PBSA) method (Homeyer and Gohlke, 2012) was employed to analyze the 100 snapshots extracted from the last 10-ns MD trajectory, resulting in the total binding free energy  $\Delta G_{\text{ttl}}$  of simulated complex, which can be expressed as follows:

$$\Delta G_{\text{ttl}} = \Delta E_{\text{int}} + \Delta D_{\text{dolv}} \quad (1)$$

where  $\Delta E_{\text{int}}$  is the intermolecular interaction energy between the EGFR and MIG6<sup>segment 2</sup> peptide and calculated using force field approach, and  $\Delta D_{\text{dolv}}$  is the desolvation free energy due to peptide

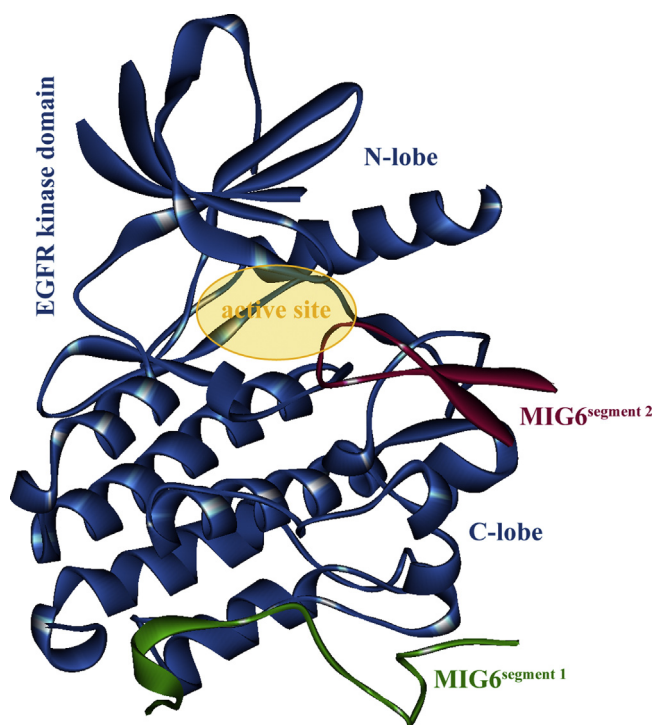


Fig. 1. The complex crystal structure of EGFR kinase domain with MIG6<sup>segment 1</sup> and MIG6<sup>segment 2</sup> (PDB: 4zjv).

binding, which can be computed by numerical solution of nonlinear Poisson–Boltzmann equation and surface area model. Here, entropy effect was not considered due to the high computational demands.

### 2.3. Computational alanine scanning

Computational alanine scanning (CAS) (Kortemme et al., 2004) has been widely used to identify hot-spot residues at protein–protein/peptide complex interface. Here, we employed CAS to detect the residue importance of MIG6<sup>segment 2</sup> peptide binding to EGFR kinase domain. In the procedure, each residue in the peptide was virtually mutated to chemically neutral alanine and then calculated peptide binding free energy change  $\Delta\Delta G$  upon the mutation:

$$\Delta\Delta G = \Delta G_{\text{ttl}}^{\text{mt}} - \Delta G_{\text{ttl}}^{\text{wt}} \quad (2)$$

where the  $\Delta G_{\text{ttl}}^{\text{wt}}$  and  $\Delta G_{\text{ttl}}^{\text{mt}}$  are the total binding free energies of wide-type and mutant peptides to EGFR, respectively, which can be calculated using MD simulation and MM/PBSA analysis, as described above.

### 2.4. Binding assay

Peptides were synthesized using standard 9-fluorenyl methoxycarbonyl (Fmoc) solid phase chemistry. Phosphotyrosine was directly incorporated as its  $N_{\alpha}$ -fluorenylmethoxycarbonyl-*O*-phosphate-*L*-tyrosine derivative. The peptides were then purified by RP-HPLC C18 columns, and were confirmed by mass spectrometry and amino acid analysis. A protocol modified from previous works was used to perform peptide binding assay (Zhang et al., 2007b; Yu et al., 2016). Briefly, fluorescence anisotropy analysis was measured using a PerkinElmer fluorimeter. Fluorescence titration was carried out with unlabeled kinase protein and N-terminally labeled peptide in a buffer (10 mM Tris–HCl, 25 mM NaCl and 2 mM DTT). The titration curves were fitted with MicroCal software package. Each assay was performed for duplicate.

## 3. Results and discussion

The MIG6<sup>segment 2</sup> peptide is composed of 23 amino acids (<sup>376</sup>VPCILPIIENGKKVCSTHYLLP<sup>398</sup>), folded into a two-stranded  $\beta$ -sheet in cocrystallized complex with EGFR kinase domain

(Fig. 1). A recent study found that phosphorylation of intact MIG6 protein at Tyr394 and Tyr395 residues is essential for binding and inhibition of EGFR (Park et al., 2015). The two residues are just within the MIG6<sup>segment 2</sup> region, and phosphorylation renders them negatively charged that promotes the two residues to separately form two salt bridges with the positively charged residues Lys875 and Lys879 of EGFR kinase domain. According to the double-headed mechanism for EGFR inhibition by MIG6 protein proposed by Zhang et al. (2007b), the MIG6<sup>segment 1</sup> first binds tightly to EGFR C-lobe to anchor MIG6 on EGFR, and then the MIG6<sup>segment 2</sup> is dynamic balance between association and dissociation with EGFR activation loop by phosphorylation and dephosphorylation at its Tyr394 and Tyr395 residues (Fig. 2). Thus, it is suggested that phosphorylation is the necessary but not sufficient condition for an isolated MIG6<sup>segment 2</sup> peptide binding to EGFR without MIG6<sup>segment 1</sup> assistance.

Here, the complex crystal structure of EGFR kinase domain with MIG6<sup>segment 2</sup> was retrieved from the PDB database (Berman et al., 2000) under accession code 4zjv (Fig. 1), in which the MIG6<sup>segment 1</sup> is also present and we just removed it, and the MIG6<sup>segment 2</sup> misses a Lys387 residue and we manually fixed it. In the crystal complex, the MIG6<sup>segment 2</sup> is doubly phosphorylated at residues Tyr394 and Tyr395 (pTyr394 and pTyr395) that can maintain in a tightly bound state with the kinase domain. The complex was then subjected to 20-ns MD simulations to remove bad atomic overlap and bond distortion involved in the structure, resulting in an equilibrium conformation. Based on the conformation computational alanine scanning was performed to characterize the residue importance of MIG6<sup>segment 2</sup> peptide. In the procedure, each residue of the peptide was virtually mutated to chemically neutral alanine and then calculated peptide binding free energy change ( $\Delta\Delta G$ ) upon the mutation. The resulting  $\Delta\Delta G$  profile of MIG6<sup>segment 2</sup> peptide is visualized in Fig. 3. As can be seen, most residues exhibit unfavorable mutation by replacing with the neutral alanine ( $\Delta\Delta G > 0$ ), indicating that the native residues of MIG6<sup>segment 2</sup> have a good compatibility with EGFR kinase domain. This is expected if considering that MIG6<sup>segment 2</sup> is optimized to well fit its cognate partner EGFR during genetic evolution. In addition, the  $\Delta\Delta G$  values vary significantly over the 23 MIG6<sup>segment 2</sup> residues; the N-terminal and central residues can only address moderate or modest effect on peptide binding ( $\Delta\Delta G < 0.5$  kcal/mol), while the C-terminal residues contribute considerably to the binding ( $\Delta\Delta G > 0.5$  kcal/mol). In particular, the fragment ranging between

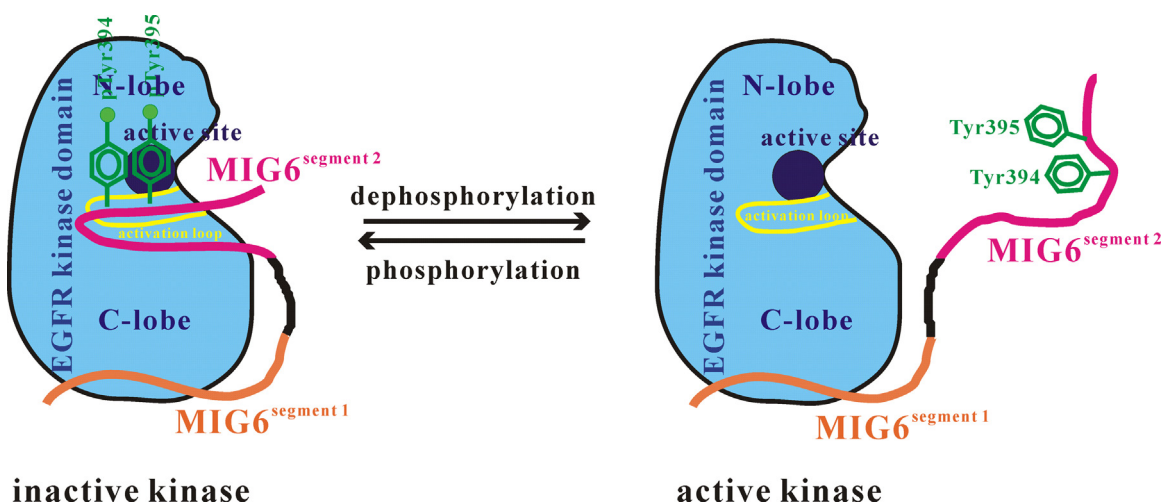


**Fig. 2.** The double-headed mechanism for EGFR inhibition by MIG6 protein proposed by Zhang et al. (2007b). The MIG6<sup>segment 1</sup> first binds tightly to EGFR C-lobe to anchor MIG6 on EGFR, and then the MIG6<sup>segment 2</sup> is dynamic balance between association and dissociation with EGFR activation loop by phosphorylation and dephosphorylation at its Tyr394 and Tyr395 residues.

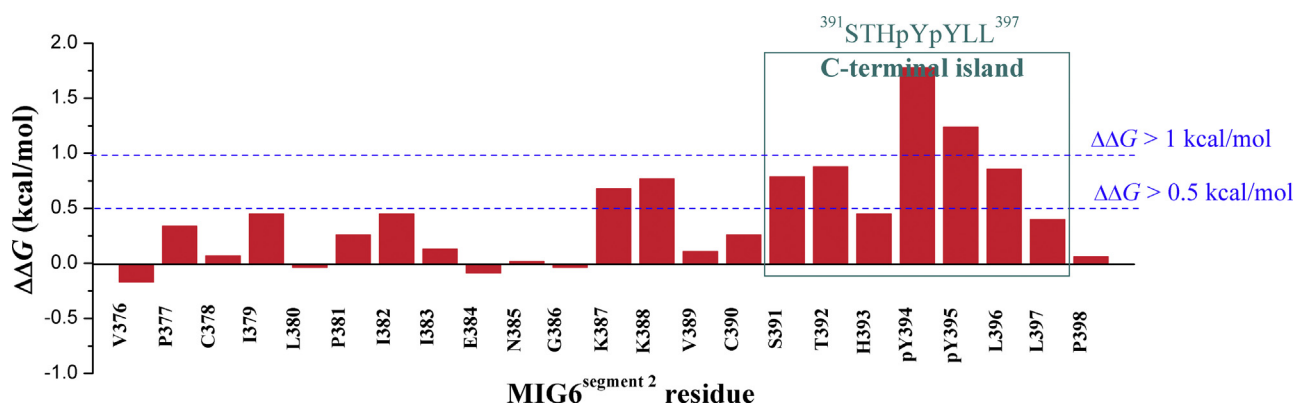


**Fig. 3.** The binding free energy change ( $\Delta\Delta G$ ) profile of 23  $\text{MIG6}^{\text{segment } 2}$  residues calculated using computational alanine scanning (Kortemme et al., 2004).  $\Delta\Delta G < 0$ : favorable mutation,  $\Delta\Delta G > 0$ : unfavorable mutation.

residues 391 and 397 ( $^{391}\text{STHpYpYLL}^{397}$ ) defines a C-terminal island, which plays a critical role in EGFR– $\text{MIG6}^{\text{segment } 2}$  interaction. As might be expected, the two phosphorylated residues pTyr394 and pTyr395 are just located within the island and confer strong affinity for the EGFR– $\text{MIG6}^{\text{segment } 2}$  interaction with  $\Delta\Delta G$  values of 1.78 and 1.24 kcal/mol, respectively.

By examining the complex structure of EGFR kinase domain with  $\text{MIG6}^{\text{segment } 2}$ , the  $\text{MIG6}^{\text{segment } 2}$  peptide is folded into a two-stranded  $\beta$ -sheet structure composed of  $\beta$ -strand 1 and  $\beta$ -strand 2; the former is set apart from the kinase domain, while the latter directly contacts the domain (Fig. 4a). The C-terminal island is within the  $\beta$ -strand 2, which can effectively interact with EGFR activation loop to form anti-parallel adduct between them. In contrast, the N-terminal  $\beta$ -strand 1 is just added to the  $\beta$ -strand 2 to define a two-stranded  $\beta$ -sheet architecture for the *holo* structure of  $\text{MIG6}^{\text{segment } 2}$ . The two phosphorylated residues pTyr394 and pTyr395 in C-terminal island can form two geometrically perfect salt bridges (lengths = 4.62 and 4.11 Å) with the positively charged residues Lys879 and Lys875 of EGFR kinase domain, respectively (Fig. 4b). This is in line with the binding free energy change ( $\Delta\Delta G$ ) profile that mutation of the two residues would cause a large binding free energy loss for the EGFR– $\text{MIG6}^{\text{segment } 2}$  complex.

The total binding free energy ( $\Delta G_{\text{ttl}}$ ) of dephosphorylated  $\text{MIG6}^{\text{segment } 2}$  peptide (MSP) and its derivative versions to EGFR kinase domain are listed in Table 1. By comparing between these peptides it is found that the unmodified MSP can only interact weakly with EGFR ( $\Delta G_{\text{ttl}} = -3.7$  kcal/mol); separated phosphorylation at residues pTyr394 (MSP<sup>p394</sup>) or pTyr395 (MSP<sup>p395</sup>) can moderately improve peptide binding free energy ( $\Delta G_{\text{ttl}} = -7.8$  or  $-5.6$  kcal/mol), while simultaneous phosphorylation of the two residues (MSP<sup>p394,p395</sup>) can substantially promote the binding ( $\Delta G_{\text{ttl}} = -13.4$  kcal/mol). Next, the MSP was truncated at its two ends, remaining the region  $^{391}\text{STHYLL}^{397}$  (MSP<sup>trt</sup>) corresponding to C-terminal island, which can only bind modestly to EGFR ( $\Delta G_{\text{ttl}} = -2.6$  kcal/mol) as compared to intact MSP. Similarly, the binding free energy improves moderately ( $\Delta G_{\text{ttl}} = -4.3$  or  $-3.2$  kcal/mol) upon phosphorylation of the truncated peptide at residue pTyr394 (MSP<sup>trt,p394</sup>) or pTyr395 (MSP<sup>trt,p395</sup>), while a large free energy increase ( $\Delta G_{\text{ttl}} = -8.5$  kcal/mol) is observed due to simultaneous phosphorylation of the two residues (MSP<sup>trt,p394,p395</sup>).

Next, the sequence pattern of MSP<sup>trt,p394,p395</sup> peptide ( $^{391}\text{STHpYpYLL}^{397}$ ) was optimized to obtain new peptides with improved affinity. Evidently, the two phosphorylatable residues Tyr394 and Tyr395 in the peptide should be fixed across the

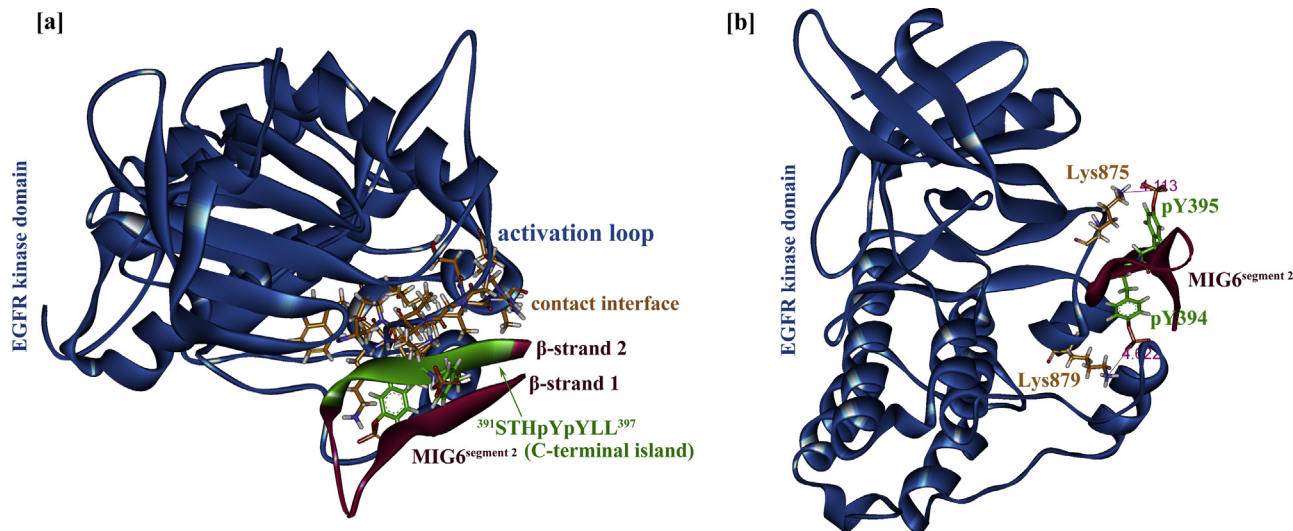


**Fig. 4.** [a] The  $\text{MIG6}^{\text{segment } 2}$  is folded into a two-stranded  $\beta$ -sheet structure composed of  $\beta$ -strand 1 and  $\beta$ -strand 2; the former is set apart from EGFR kinase domain, while the latter interacts directly with the domain. [b] The phosphonated residues pTyr394 and pTyr395 of  $\text{MIG6}^{\text{segment } 2}$  can form two strong salt bridges (lengths = 4.62 and 4.11 Å) with the positively charged residues Lys879 and Lys875 of EGFR kinase domain, respectively.

**Table 1**The binding free energies of different derivative versions of MIG6<sup>segment 2</sup> peptide to EGFR kinase domain.

Name	Treatment	Sequence	$\Delta G_{\text{int}}$ (kcal/mol)
MSP	/	<sup>376</sup> VPCILPIIENGKKVCSTHYLLP <sup>398</sup>	-3.7
MSP <sup>p394</sup>	pTyr394	<sup>376</sup> VPCILPIIENGKKVCSTHpYLLP <sup>398</sup>	-7.8
MSP <sup>p395</sup>	pTyr395	<sup>376</sup> VPCILPIIENGKKVCSTHpYLLP <sup>398</sup>	-5.6
MSP <sup>p394,p395</sup>	pTyr394, pTyr395	<sup>376</sup> VPCILPIIENGKKVCSTHpYpYLLP <sup>398</sup>	-13.4
MSP <sup>trt</sup>	Truncation	<sup>391</sup> STHYLL <sup>397</sup>	-2.6
MSP <sup>trt,p394</sup>	Truncation, pTyr394	<sup>391</sup> STHpYLL <sup>397</sup>	-4.3
MSP <sup>trt,p395</sup>	Truncation, pTyr395	<sup>391</sup> STHyPpYLL <sup>397</sup>	-3.2
MSP <sup>trt,p394,p395</sup>	Truncation, pTyr394, pTyr395	<sup>391</sup> STHpYpYLL <sup>397</sup>	-8.5

optimization due to their critical role in kinase–peptide binding, thus remaining five optimizable residues Ser391, Thr392, His393, Leu396 and Leu397. Considering that it is very computationally exhaustive to systematically search against the whole combination space of 20 amino acid candidates at the five residues, we herein only performed mutation independently at each of these sites, and also only considered representative amino acid types (but not all the 20 natural amino acids) in the mutation. This simplification is reasonable since peptide binding to protein receptor follows the IBS (independent binding of side-chains) hypothesis (Parker et al., 1994). We selected eight representative amino acids (Gly, Val, Ile, Asn, Phe, Trp, Lys and Glu) from the 20 natural amino acids, which cover a wide range of physicochemical properties including small, bulky, hydrophobic, hydrophilic, aromatic, positively charged and negatively charged. Subsequently, each of the five optimizable residues was computationally mutated to the eight representative amino acids one-by-one, and the peptide binding free energy change  $\Delta\Delta G$  upon the mutation was then calculated, resulting in a  $5 \times 8$  mutation energy profile. As can be seen in Fig. 5a, most substitution mutations can only influence peptide binding moderately, and most mutations have unfavorable effect on the binding. This is in line with the binding free energy change profile of MIG6<sup>segment 2</sup> determined by computational alanine scanning. In particular, the replacement of Thr392 and Leu396 by Trp can cause large free energy loss in peptide binding ( $\Delta\Delta G > 1$  kcal/mol). Structural examination revealed that the bulky Trp side chain would introduce intensive atomic collisions and bad overlaps at the tightly packed kinase–peptide interface that are responsible for the free energy penalty. In addition, either positively charged Lys or negatively charged Glu seems also unfavorable to peptide binding.

In fact, the interface is primarily nonpolar and presence of the charged amino acids would thus impair the established hydrophobic forces and van der Waals interactions across the native complex interface.

On the other side, two mutations were identified to be energetically favorable for peptide binding, including Thr392Ile and His393Asn (Fig. 5b), which can improve peptide affinity considerably with  $\Delta\Delta G < -0.5$  kcal/mol. The two mutations were computationally modeled in the complex structure of EGFR kinase domain with wild-type peptide to construct mutant structures. It is evident in Fig. 6a that the two mutations are close to EGFR activation loop and a number of nonbonded interactions across the kinase–peptide interface can be established due to the mutations. As can be seen in Fig. 6b, the Thr392Ile mutation replaces the polar amino acid Thr by a nonpolar Ile at peptide residue 392, forming hydrophobic contacts with the nonpolar and/or aromatic residues Trp880 and Pro887 of EGFR, while the His393Asn mutation can introduce a geometrically satisfactory hydrogen bond with the backbone oxygen of kinase residue Ala772.

Guided by above computational findings we herein designed three mutated versions of wild-type MSP<sup>trt,p394,p395</sup> peptide (STHpYpYLL), namely, MSP<sup>trt,p394,p395,T392I</sup> (<sup>391</sup>SIHpYpYLL<sup>397</sup>), MSP<sup>trt,p394,p395,H393N</sup> (<sup>391</sup>STNpYpYLL<sup>397</sup>), and MSP<sup>trt,p394,p395,T392I,H393N</sup> (<sup>391</sup>SINpYpYLL<sup>397</sup>). The MSP<sup>trt,p394,p395,T392I</sup> and MSP<sup>trt,p394,p395,H393N</sup> are the mutants of MSP<sup>trt,p394,p395</sup> with single-point mutation of Thr392Ile and His393Asn, respectively, while the MSP<sup>trt,p394,p395,T392I,H393N</sup> is the double mutant at the two residues. For comparison purpose the dephosphonated version (MSP<sup>trt</sup>) of wild-type MSP<sup>trt,p394,p395</sup> was also discussed. The binding free energies of these peptides to EGFR kinase domain were calculated

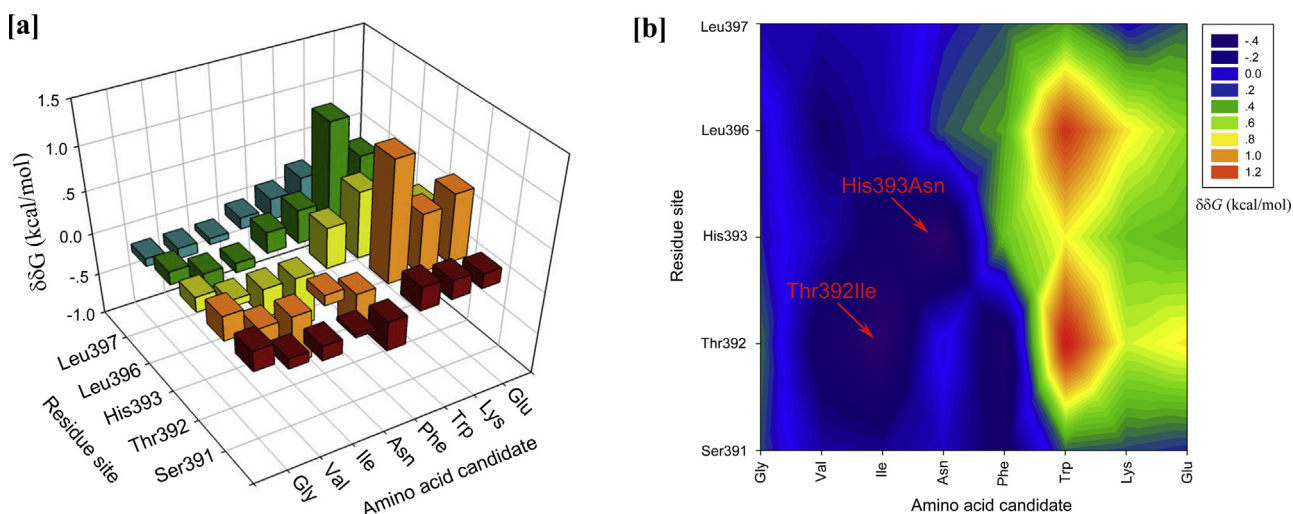


**Fig. 5.** The binding free energy change ( $\Delta\Delta G$ ) profile of MIG6<sup>segment 2</sup> by mutating five optimizable residues Ser391, Thr392, His393, Leu396 and Leu397 to eight representative amino acid candidates Gly, Val, Ile, Asn, Phe, Trp, Lys and Glu.  $\Delta\Delta G < 0$ : favorable mutation,  $\Delta\Delta G > 0$ : unfavorable mutation. [a] Histogram. [b] Counter plot.

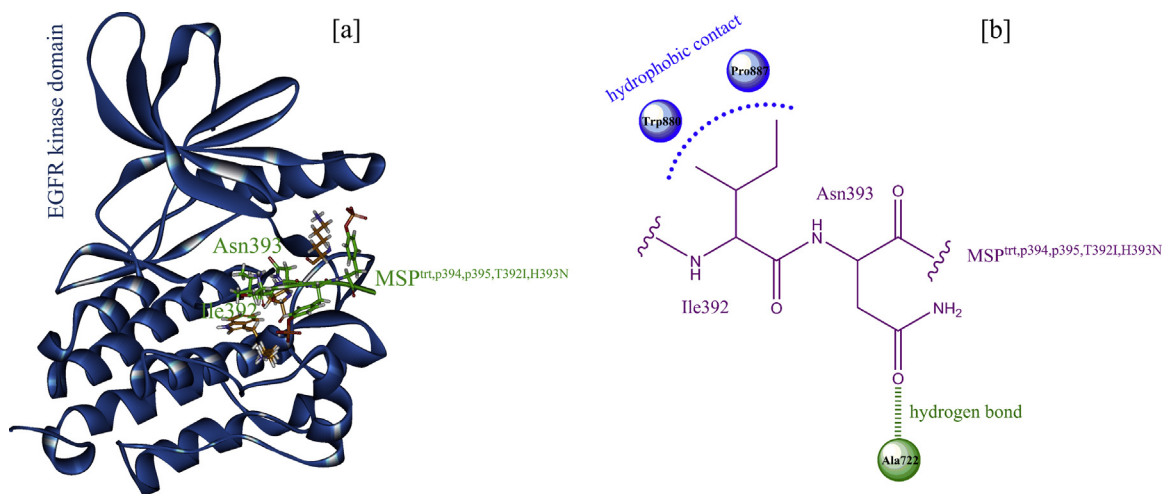


**Fig. 6.** [a] The computationally modeled complex structure of EGFR kinase domain with MSP<sup>trt,p394,p395,T392I,H393N</sup> peptide. [b] Schematic representation of hydrophobic contact and hydrogen bond involving the mutated residues Ile392 and Asn393 of peptide.

**Table 2**  
The calculated binding free energies  $\Delta G_{\text{ttl}}$  and experimental affinities  $K_d$  of truncated MIG6<sup>segment 2</sup> peptide as well as its three mutants and dephosphonated version to EGFR kinase domain.

Name	Treatment	Sequence	$\Delta G_{\text{ttl}}$ (kcal/mol)	$K_d$ ( $\mu\text{M}$ )
MSP <sup>trt</sup>	Truncation	391STHYLL <sup>397</sup>	-2.6	n.d. <sup>a</sup>
MSP <sup>trt,p394,p395</sup>	Truncation, pTyr394, pTyr395	391STHpYpYLL <sup>397</sup>	-8.5	276.0 $\pm$ 22.4
MSP <sup>trt,p394,p395,T392I</sup>	Truncation, pTyr394, pTyr395, Thr392Ile	391SIHpYpYLL <sup>397</sup>	-9.2	n.a. <sup>b</sup>
MSP <sup>trt,p394,p395,H393N</sup>	Truncation, pTyr394, pTyr395, His393Asn	391STNpYpYLL <sup>397</sup>	-11.4	n.a. <sup>b</sup>
MSP <sup>trt,p394,p395,T392I,H393N</sup>	Truncation, pTyr394, pTyr395, Thr392Ile, His393Asn	391SINpYpYLL <sup>397</sup>	-12.1	54.7 $\pm$ 4.8

<sup>a</sup> n.d., not determined.

<sup>b</sup> n.a., not assayed.

using MD simulations and MM/PBSA analysis (listed in Table 2). As expected, MSP<sup>trt</sup> only binds weakly to the kinase with  $\Delta G_{\text{ttl}} = -2.6$  kcal/mol, and the phosphonation at Y394 and Y395 (MSP<sup>trt,p394,p395</sup>) can substantially improve peptide affinity with  $\Delta G_{\text{ttl}} = -8.5$  kcal/mol. The two designed single-point mutants (MSP<sup>trt,p394,p395,T392I</sup> and MSP<sup>trt,p394,p395,H393N</sup>) as well as the double-point mutant (MSP<sup>trt,p394,p395,T392I,H393N</sup>) receive a further affinity increase, although the effect of mutations on peptide binding seems to be moderate ( $\Delta G_{\text{ttl}} = -9.2$ ,  $-11.4$  and  $-12.1$  kcal/mol). The theoretically predicted affinity improvement can be substantiated by peptide binding assay, where the dephosphonated version MSP<sup>trt</sup>, phosphonated peptide MSP<sup>trt,p394,p395</sup> and the double-point mutant MSP<sup>trt,p394,p395,T392I,H393N</sup> were measured *in vitro* by fluorescence anisotropy analysis. Consequently, no binding was assayed for MSP<sup>trt</sup>, while modest and moderate affinities were observed to MSP<sup>trt,p394,p395</sup> and MSP<sup>trt,p394,p395,T392I,H393N</sup> with  $K_d = 276.0$  and  $54.7 \mu\text{M}$ , respectively. The two designed peptides can be considered as promising lead entities to develop potent EGFR targeting agents against lung cancer.

## Acknowledgement

This work was supported by the Taizhou Municipal Hospital.

## References

- Berman, H.M., Westbrook, J., Feng, Z., Gilliland, G., Bhat, T.N., Weissig, H., Shindyalov, I.N., Bourne, P.E., 2000. The protein data bank. *Nucleic Acids Res.* 28, 235–242.  
Bethune, G., Bethune, D., Ridgway, N., Xu, Z., 2010. Epidermal growth factor receptor (EGFR) in lung cancer: an overview and update. *J. Thorac. Dis.* 2, 48–51.

- Darden, T., York, D., Pedersen, L., 1993. Particle Mesh Ewald: an N-Log(N) method for Ewald sums in large systems. *J. Chem. Phys.* 98, 10089–10092.  
Duan, Y., Wu, C., Chowdhury, S., Lee, M.C., Xiong, G., Zhang, W., Yang, R., Cieplak, P., Luo, R., Lee, T., Caldwell, J., Wang, J., Kollman, P., 2003. A point-charge force field for molecular mechanics simulations of proteins based on condensed-phase quantum mechanical calculations. *J. Comput. Chem.* 24, 1999–2012.  
Ferby, I., Reschke, M., Kudlacek, O., Knyazev, P., Pantè, G., Amann, K., Sommergruber, W., Kraut, N., Ullrich, A., Fässler, R., Klein, R., 2006. Mig-6 is a negative regulator of EGF receptor-mediated skin morphogenesis and tumor formation. *Nat. Med.* 12, 568–573.  
Hackel, P.O., Gishizky, M., Ullrich, A., 2001. Mig-6 is a negative regulator of the epidermal growth factor receptor signal. *Biol. Chem.* 382, 1649–1662.  
Homeyer, N., Gohlke, H., 2012. Free energy calculations by the molecular mechanics Poisson–Boltzmann surface area method. *Mol. Inf.* 31, 114–122.  
Izumchenko, E., Sidransky, D., 2015. Understanding the MIG6-EGFR signaling axis in lung tumorigenesis. *Cancer Discov.* 5, 472–474.  
Jorgensen, W.L., Chandrasekhar, J., Madura, J.D., Impey, R.W., Klein, M.L., 1983. Comparison of simple potential functions for simulating liquid water. *J. Chem. Phys.* 79, 926–935.  
Kortemme, T., Kim, D.E., Baker, D., 2004. Computational alanine scanning of protein–protein interfaces. *STKE* 2004, pl2.  
Kim, T.H., Yoo, J.Y., Kim, H.I., Gilbert, J., Ku, B.J., Li, J., Mills, G.B., Broaddus, R.R., Lydon, J.P., Lim, J.M., Yoon, H.G., Jeong, J.W., 2014. Mig-6 suppresses endometrial cancer associated with Pten deficiency and ERK activation. *Cancer Res.* 74, 7371–7382.  
Lemmon, M.A., Schlessinger, J., 2010. Cell signaling by receptor tyrosine kinases. *Cell* 141, 1117–1134.  
Maity, T.K., Venugopalan, A., Linnoila, I., Cultraro, C.M., Giannakou, A., Nemati, R., Zhang, X., Webster, J.D., Ritt, D., Ghosal, S., Hoschuetzky, H., Simpson, R.M., Biswas, R., Politi, K., Morrison, D.K., Varmus, H.E., Guha, U., 2015. Loss of MIG6 accelerates initiation and progression of mutant epidermal growth factor receptor-driven lung adenocarcinoma. *Cancer Discov.* 5, 534–549.  
Moonrin, N., Songtawee, N., Rattanabunyong, S., Chunsriviro, S., Mokmak, W., Tongsima, S., Choowongkamon, K., 2015. Understanding the molecular basis of EGFR kinase domain/MIG-6 peptide recognition complex using computational analyses. *BMC Bioinform.* 16, 103.  
Parker, K.C., Bednarek, M.A., Coligan, J.E., 1994. Scheme for ranking potential HLA-A2 binding peptides based on independent binding of individual peptide side-chains. *J. Immunol.* 152, 163–175.

- Park, E., Kim, N., Ficarro, S.B., Zhang, Y., Lee, B.I., Cho, A., Kim, K., Park, A.K., Park, W.Y., Murray, B., Meyerson, M., Beroukhir, R., Marto, J.A., Cho, J., Eck, M.J., 2015. Structure and mechanism of activity-based inhibition of the EGF receptor by Mig6. *Nat. Struct. Mol. Biol.* 22, 703–711.
- Ryckaert, J.P., Ciccotti, G., Berendsen, H.J.C., 1977. Numerical integration of the Cartesian equations of motion of a system with constraints: molecular dynamics of *n*-alkanes. *J. Comput. Phys.* 23, 327–341.
- Steinbrecher, T., Latzer, J., Case, D.A., 2012. Revised AMBER parameters for bioorganic phosphates. *J. Chem. Theory Comput.* 8, 4405–4412.
- Wendt, M.K., Williams, W.K., Pascuzzi, P.E., Balanis, N.G., Schiemann, B.J., Carlin, C.R., Schiemann, W.P., 2015. The antitumorigenic function of EGFR in metastatic breast cancer is regulated by expression of Mig6. *Neoplasia* 17, 124–133.
- Yu, X.D., Guo, A.F., Zheng, G.H., Yang, X.W., Shi, P.C., 2016. Design and optimization of peptide ligands to target breast cancer-positive HER2 by grafting and truncation of MIG6 peptide. *Int. J. Pept. Res. Ther.* doi:<http://dx.doi.org/10.1007/s10989-015-9501-9> (Epub ahead of press).
- Zhang, X., Gureasko, J., Shen, K., Cole, P.A., Kuriyan, J., 2006. An allosteric mechanism for activation of the kinase domain of epidermal growth factor receptor. *Cell* 125, 1137–1149.
- Zhang, Y.W., Staal, B., Su, Y., Swiatek, P., Zhao, P., Cao, B., Resau, J., Sigler, R., Bronson, R., Vande Woude, G.F., 2007a. Evidence that MIG-6 is a tumor-suppressor gene. *Oncogene* 26, 269–276.
- Zhang, X., Pickin, K.A., Bose, R., Jura, N., Cole, P.A., Kuriyan, J., 2007b. Inhibition of the EGF receptor by binding of MIG6 to an activating kinase domain interface. *Nature* 450, 741–744.